An Optimal Vector-Network-Analyzer Calibration Algorithm

Dylan F. Williams, *Fellow, IEEE*, Jack C. M. Wang, and Uwe Arz, *Member, IEEE*

***Abstract*—We present an iterative algorithm for calibrating vector network analyzers based on orthogonal distance regression. The algorithm features a robust, yet efficient, search algorithm, an error analysis that includes both random and systematic errors, a full covariance matrix relating calibration and measurement errors, 95% coverage factors, and an easy-to-use user interface that supports a wide variety of calibration standards. We also discuss evidence that the algorithm outperforms the *MultiCal* software package in the presence of measurement errors and accurately estimates the uncertainty of its results.**

***Index Terms*—Calibration, measurement, scattering parameter, uncertainty, vector network analyzer (VNA).**

I. Introduction

We present an iterative algorithm, which we first introduced in [1], for vector-network-analyzer (VNA) calibration based on orthogonal distance regression. In [1], we showed that, in the presence of random measurement errors, this new algorithm outperforms the multiline thru-reflect-line (TRL) VNA calibration algorithm of [2] implemented in the National Institute of Standards and Technology's (NIST), Boulder, CO, popular *MultiCal* software package.[1] We also showed that the new algorithm accurately estimates the uncertainty of its results.

Here, we will describe this new algorithm in detail, and present many aspects of its operation not touched on in [1]. We will describe the robust search strategy employed by the algorithm, and the wide variety of standards that the algorithm supports (see the Appendix). We will also describe the innovative strategy employed by the new algorithm to solve one-tier calibration problems and to find the scattering parameters of the device-under-test (DUT).

We will discuss how the algorithm estimates the uncertainty of its results using residual deviations of the measurements from the VNA calibration model. We will also discuss the mechanism supported by the algorithm for adding systematic errors that are not captured by the residual deviations of the measurements from the VNA calibration model into the overall uncertainty estimates.

Finally, we will discuss the algorithm's uncertainty estimates, which we chose to express as a covariance matrix relating uncertainties in the calibration *and* the measurements of the DUT. This covariance matrix includes the correlations between all of the measurements and all of the calibration parameters, information that is essential for performing rigorous analyses of many on-wafer problems in which both the probes and DUT must be characterized from measurements.

We will discuss not only how we assemble this covariance matrix from separate solutions of the calibration and DUT problems and from electrical models capturing the systematic errors, but also how we determine the numbers of degrees of freedom associated with each of these solutions, and develop appropriate coverage factors.

II. Prior Work

The iterative approaches of [3] and [4] were the first to offer alternative solutions to closed-form VNA calibrations. The two approaches were based, respectively, on nonlinear least-squares solutions to the conventional VNA and six-port calibration problems. While these iterative approaches are slower and less compact than their closed-form counterparts, they are designed for optimal performance in the presence of measurement errors.

Reference [5] extended the approaches of [3] and [4] to a 16-term error model and developed error estimates. Reference [6] applied the nonlinear least-squares approach to nonlinear VNAs.

We later adapted the nonlinear least-squares solution of [3] to the characterization of planar coupled transmission lines in [7]–[10]. In this case, the least-squares solution was obtained using the orthogonal distance regression algorithm implemented in ODRPACK [11]. The algorithms of [7]–[10] took advantage of the ability of ODRPACK to determine confidence intervals for the results directly from measurement data.

In this paper, we discuss the details of the implementation of the new VNA calibration algorithm described in [1]. Like [7]–[10], this algorithm is based on orthogonal distance regression, and is a culmination of the algorithms developed in [3] and [7]–[10]. Unlike its predecessors, this new algorithm takes full advantage of the ability of orthogonal distance regression to separate and treat errors in the measurements and standard definitions, and incorporates a mechanism for adding systematic errors into its overall uncertainty estimates.

Manuscript received April 16, 2003.

D. F. Williams is with the Electromagnetic Fields Division, National Institute of Standards and Technology, Boulder, CO 80305 USA.

J. C. M. Wang is with the Statistical Engineering Division, National Institute of Standards and Technology, Boulder, CO 80305 USA.

U. Arz is with the Electricity Division, Physikalisch-Technische Bundesanstalt, 38116 Braunschweig, Germany.

Digital Object Identifier 10.1109/TMTT.2003.819211

[1]*MultiCal* may be obtained online. [Online]. Available: www.boulder.nist.gov/micro. *MultiCal* is a trademark of the National Institute of Standards and Technology (NIST), Boulder, CO.

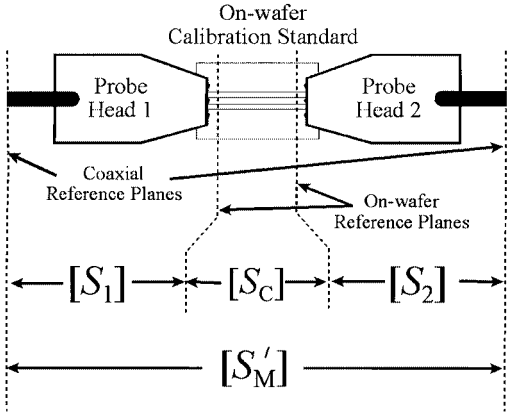

Fig. 1. Two-tier on-wafer calibration problem (from [1]).

III. Two-Tier Calibration Problem

Fig. 1 shows the basic second-tier on-wafer measurement problem that we address with the new calibration algorithm. The matrices $[S_1]$ and $[S_2]$ contain the scattering parameters of the two microwave ground–signal–ground probe heads we wish to characterize. (The matrices $[S_1]$ and $[S_2]$ would contain the scattering parameters of the adapters if we were characterizing a fixture.) The matrix $[S_C]$ contains the scattering parameters of the on-wafer calibration standard contacted by the probes. The elements of $[S'_M]$ are the scattering parameters of the cascade of the left probe head, calibration standard, and right probe head, as measured by the network analyzer at the coaxial reference planes indicated in this figure. Here, the prime indicates that $[S'_M]$ is a measured, rather than a calculated, quantity. The objective of the calibration is to determine the scattering-parameter matrices $[S_1]$ and $[S_2]$ of two probe heads from measurements $[S'_M]$ of the probes and known on-wafer calibration standards.

In the multiline TRL calibration, the on-wafer standards consist of a short "thru" line, a set of additional on-wafer transmission lines of differing lengths, and a symmetric "reflect" [12]. In other calibration methods, the lines and/or reflect may be replaced by a variety of previously characterized terminations or other two-port calibration standards.

IV. Calibration Algorithm

The orthogonal-distance-regression algorithm implemented in ODRPACK [11] finds an optimal solution for β of the n equations

$$y_i = f_i(x_i + \delta_i, \beta) - \varepsilon_i \tag{1}$$

where the subscript i corresponds to the ith one of the n "observations." The f_i are functions relating the measurements y_i to the unknown vector β and the explanatory variables x_i. ε_i and δ_i are the errors we wish to minimize in y_i and x_i.

To solve the calibration problem of Fig. 1, we set elements of the measurement vectors y_i to the real and imaginary parts of the elements of the measured scattering-parameter matrices $[S'_M]$ of the two probes and calibration standard. The vector β contains the unknowns we wish to determine. We assigned elements of β to the real and imaginary parts of the elements of the scattering-parameter matrices $[S_1]$ and $[S_2]$ of the probe heads and, when appropriate, the effective dielectric constant ε_{eff} of the on-wafer transmission-line standards, the unknown reflection coefficient Γ_r of the symmetric on-wafer reflect standards, and the reflection and transmission coefficients of the reciprocal adapter calibration standard (see the Appendix).

The vectors x_i contain sets of "explanatory" variables for each observation. We use them to describe measurements or models defining the scattering parameters of calibration standards, setting elements of x_i to the real and imaginary parts of the elements of the scattering-parameter matrix $[S_C]$ of the calibration standard. This strategy allows the algorithm to accommodate imperfectly characterized calibration standards.

The optimal solution for β is found by determining the vector η that minimizes

$$s(\eta) = \sum_{i=1}^{n} \left(\varepsilon_i^T w_{\varepsilon_i} \varepsilon_i + \delta_i^T w_{\delta_i} \delta_i\right) \equiv G(\eta)^T \Omega G(\eta) \tag{2}$$

subject to the constraints in (1). In (2), the matrices w_ε and w_δ are weights, $\eta^T \equiv (\beta^T, \delta_1^T, \ldots, \delta_n^T)$, $G(\eta)^T \equiv (\varepsilon_1^T, \ldots, \varepsilon_n^T, \delta_1^T, \ldots, \delta_n^T)$, the superscript T indicates the transpose, and

$$\Omega \equiv \begin{bmatrix} w_{\varepsilon 1} & & & \\ & \ddots & & \\ & & w_{\delta 1} & \\ & & & \ddots \end{bmatrix}. \tag{3}$$

Finally, ODRPACK estimates Σ_β, the covariance matrix corresponding to the elements of the solution vector β, from

$$\Sigma_\eta \equiv \begin{bmatrix} \Sigma_\beta & \Sigma_{\beta\delta} \\ \Sigma_{\delta\beta} & \Sigma_\delta \end{bmatrix} = \hat{\sigma}^2 \left[J^T \Omega J\right]^{-1} \tag{4}$$

where $\hat{\sigma}^2 \equiv (s(\hat{\eta})/\mu)$ is the estimated residual variance. Here, μ, the number of degrees of freedom, is the number of observations minus the number of parameters being estimated, and the jkth element of the Jacobian matrix $\boldsymbol{J}$ is equal to $\partial G_j/\partial \eta_k$ evaluated at $\hat{\eta}$.

In our implementation of the on-wafer calibration algorithm, we allow the user to specify uniform weights. We also allow the user to set w_ε and w_δ equal to estimates of the inverse of user-supplied block-diagonal covariance matrices Σ_y and Σ_x describing the uncertainties in y_i and x_i. This improves the estimate of the unknowns in the vector β over that obtained with uniform weighting [11]. When the x_i's are fixed, w_δ set to 0, and Σ_y are diagonal, minimizing (2) in this way corresponds to "chi-square" fitting [13].

V. Algorithm Performance—An On-wafer Test Case

In [1], we used a Monte Carlo simulation of a second-tier on-wafer TRL calibration to compare the performance of our new orthogonal-distance-regression algorithm to the algorithm of [2] as implemented in *MultiCal*. While neither algorithm showed statistically significant bias in its solutions, we found that our new algorithm outperformed the algorithm of [2] in the presence of measurement errors. Fig. 2 illustrates this key result of [1].

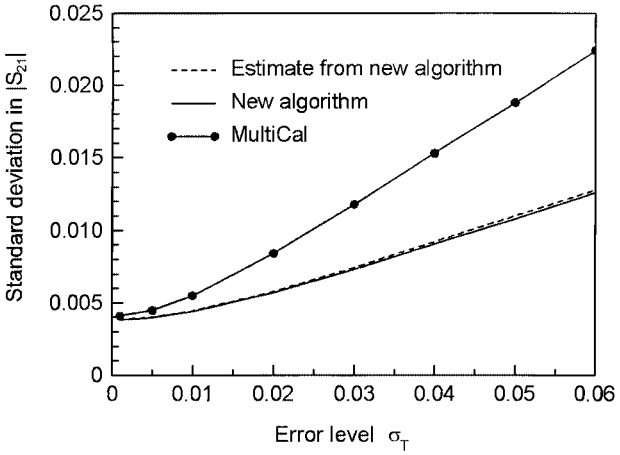

Fig. 2. Relative performance of the two algorithms in a Monte Carlo simulation. We compared the performance of the two algorithms with identical, but noisy data sets.

To generate this figure, we first constructed a set of perfect measurements for a second-tier on-wafer TRL calibration. We added random Gaussian errors with a standard deviation of 0.01 and σ_T to the real and imaginary parts of the reflection and transmission coefficients of the simulated measurements, respectively. We then used the two algorithms to estimate the simulated values with the set of noisy measurements. Finally, we compared the calibration parameters determined by the two algorithms to their true values used in the simulation.

Fig. 2 plots the standard deviation of the errors in the magnitude of the first error box's transmission coefficient $S_{1,21}$ that we obtained with the two algorithms. The figure shows that, while the two algorithms do equally good jobs of estimating solutions at low levels of measurement error, the new algorithm does a better job of estimating the true value of the transmission coefficient of the error box in the presence of higher levels of measurement error.

This figure also compares the average value of the standard uncertainty estimated by the new algorithm in the experiment (the dashed curve in the figure) to the actual standard deviation of its results. The good agreement demonstrates the ability of the new algorithm to estimate its own uncertainty.

Reference [1] statistically quantifies these and other related results. In particular, it shows that we can state with great statistical certainty that the new algorithm outperforms the algorithm of [2], and that we can have confidence in the new algorithm's uncertainty estimates.

VI. One-Tier Calibration Problem

We use the 12-to-8-term reduction [14], [15] to solve one-tier VNA calibration problems. That is, we use isolation and switch-term measurements to first correct the raw VNA measurements for the isolation and switch-term errors, and then use orthogonal distance regression to solve for the remaining two error boxes $[S_1]$ and $[S_2]$ that define the calibration problem. The advantage of this approach is that only two new terms, the real and imaginary parts of the ratio of the forward to the reverse transmission coefficient of $[S_2]$, are required to find a solution [15]. This both increases the efficiency and robustness of the search algorithm, and improves the reliability of the algorithm's uncertainty estimates.

There is a disadvantage to this approach: we are unable to make use of repeated measurements of the isolation and switch terms. However, the switch terms themselves depend only on the instrumentation, not the calibration, calibration standards, or standard definitions that we apply. They are also small and extremely stable. Thus, we lose little information by not including repeated measurements of the switch terms.

Furthermore, even though the algorithm makes no use of repeated isolation and switch-term measurements, it can still provide good estimates of the uncertainty due to poorly characterized isolation or switch terms from the measurement residuals. This is because errors in the isolation or switch terms manifest themselves as a lack of fit of the isolation and switch-term corrected measurements to the remaining eight-term calibration error model, and are thus automatically included in the algorithm's uncertainty estimates. Thus, we felt that the advantages of using the 12-to-8-term reduction to solve one-tier calibrations outweighed its disadvantages.

VII. Search Strategy

We have found that most calibration problems are readily solved when accurate solution estimates are available as starting points. However, any iterative search algorithm can have difficulty finding solutions without good starting points, especially as the number of parameters in the solution vector β increases. TRL calibrations are particularly challenging, as they require solving for the effective dielectric constant ε_{eff} and the reflection coefficient Γ_r of the reflect standard. One-tier calibrations and calibrations with DUTs also increase the number of unknowns, and can complicate the process of finding a solution when accurate starting estimates are not available.

With these difficulties in mind, we developed an efficient and robust solution strategy to handle poor starting estimates.

Our solution strategy is based on building up the complete solution in small steps. For one-tier calibrations, we begin by finding starting estimates for the ratio of the forward to the reverse transmission coefficient of $[S_2]$ from the most reliable standard available, the thru line. If a thru line is not available in the calibration, we use a reciprocal adapter; if neither a thru, nor a reciprocal adapter is available, we use a line standard for the estimate.

When the calibration must estimate the effective dielectric constant ε_{eff} of the transmission-line standards, the reflection coefficient Γ_r of a reflect standard, or the scattering parameters of a reciprocal adapter, we first apply the orthogonal-distance-regression algorithm to find approximate solutions for $[S_1]$ and $[S_2]$ with these variables fixed at their estimates. We do this because the estimates of ε_{eff}, Γ_r, and the scattering parameters of any reciprocal adapters are usually much better known than the elements of $[S_1]$ and $[S_2]$. This greatly simplifies the job of locating the global minimum.

We then use these approximate solutions for $[S_1]$ and $[S_2]$ based on the fixed values of ε_{eff}, Γ_r, and the scattering parameters of any reciprocal adapters as starting points for

TABLE I
SOLUTION TIMES FOR A TYPICAL TRL CALIBRATION WITH DIFFERENT SOLUTION STRATEGIES

Used MultiCal start estimates ?	First pass with fixed ε_{eff} and Γ_r ?	Overall solution time
yes	no	26 seconds
no	yes	38 seconds
no	no	45 seconds

an accurate solution of the calibration problem in which all of the calibration parameters are allowed to vary. This usually results in a faster and more robust solution than trying to solve for all of the calibration parameters in one step. Of course, if the calibration does not need to solve for ε_{eff}, Γ_r, or the scattering parameters of a reciprocal adapter, we solve for $[S_1]$ and $[S_2]$ directly.

If the algorithm does not converge properly or the residual standard deviation exceeds a user-supplied maximum value, we automatically invoke a robust search algorithm. In this event, we repeat the entire process with 15 different starting values. These starting values include three different transmission coefficients of $[S_1]$ with magnitude near one spread over one-half of the Smith chart, five different transmission coefficients of $[S_2]$ with magnitude near one spread over the four quadrants of the Smith chart, and small values of reflection coefficient. We then pick the solution with the lowest overall residual standard deviation. While this search is time consuming, it typically only need be invoked at the first frequency point, whose solution then serves as a starting point for the ensuing frequency point, and so on.

Once the calibration problem has been solved, we fix the calibration parameters and apply orthogonal distance regression to solve for the scattering parameters of the DUT. Finally, as an option, we allow a joint calibration/DUT solution. This option allows additional information from transmissionless or reciprocal DUTs to be factored into the overall solution.

Table I summarizes how well our solution strategy functions. The table gives overall solution times for a 200-frequency-point 200-MHz–110-GHz first-tier TRL calibration using eight line standards, as solved on an 860-MHz Intel Pentium III[2] processor. We see that the shortest solution time of 26 s was obtained using *MultiCal* solutions as starting points, as one would expect.

The solution time increased to 38 s when we used the full strategy outlined above, fixing both ε_{eff} and Γ_r to their estimates during the first stage of the solution process. Attempting to solve the entire calibration problem in one step resulted in the longest solution time, 45 s. This was due at least in part to the fact that the orthogonal-distance-regression algorithm did not initially converge with this strategy, and the program was forced to invoke the lengthier search to solve for the first frequency point. Even so, in all three cases, the algorithm converged to the same solution. Although heuristic, we have encountered few situations in which this robust search strategy failed.

[2]We use trade names only to completely explain the experimental conditions. This does not constitute an endorsement by NIST or by the Physikalisch-Technische Bundesanstalt, Braunschweig, Germany. Other products may work as well or better.

VIII. MEASUREMENT UNCERTAINTIES

One of the most important capabilities of our new algorithm is its ability to determine uncertainties in the calibration and measurements based on redundant data. We express these uncertainties as covariance matrices. The diagonal elements of these covariance matrices correspond to the square of the standard uncertainties of the elements of the solution vector β, while the off-diagonal elements of these covariance matrices correspond to the covariances between the elements of β.

We first calculate covariance matrices describing measurement uncertainties in the real-imaginary coordinate system in which we solve the problem. We do not calculate these covariance matrices in a polar (magnitude-angle) coordinate system due to the difficulties of expressing uncertainties in the magnitudes and angles of small vectors.

However, we do support, as a user option, an in-phase/quadrature representation of the uncertainties that maintains most of the advantages of the more traditional magnitude-angle representation while avoiding the difficulty of expressing the uncertainties of small vectors in a magnitude-angle representation. In this in-phase/quadrature representation, we rotate the elements of the covariance matrix associated with the complex vectors forming our solution into a coordinate system aligned with the direction of each of these vectors. Thus, the first component of uncertainty in a vector in this in-phase/quadrature representation corresponds to the component of the vector's uncertainty in the direction of the vector itself, while the second component of uncertainty corresponds to the uncertainty of the vector in a direction in quadrature with (perpendicular to) the vector. If the uncertainties are much smaller than the magnitude of the vector, the in-phase uncertainty corresponds to the uncertainty in the magnitude of the vector, while the quadrature uncertainty corresponds to the uncertainty in the angle of the vector divided by its magnitude.

A. Type-A Uncertainties Derived From Measurement Residuals

We estimate type-A uncertainties in the solution from the deviations of the redundant measurements from the calibration model (the measurement residuals) using (4). These statistically derived uncertainties are often, but not always, random in nature. Loosely speaking, the residuals quantify the magnitude of the errors in the solution, the weights serve to determine their relative distribution in the measurements, and the Jacobian maps the measurement residuals into the uncertainties in the calibration solution and captures the correlations of the errors in that solution.

Recall that we solve for the calibration solution, for the DUT solution, and for the combined calibration and DUT solution separately. We are thus able to determine separate covariance matrices Σ_{CAL}, Σ_{DUT}, and $\Sigma_{\text{CAL+DUT}}$ from (4) describing the respective uncertainties in each of these solutions. (In Section VIII-D, we use these covariance matrices to estimate the effective number of degrees of freedom in the solution.)

These covariance matrices estimate uncertainty in the solution due not only to random measurement error, but also to a

number of other mechanisms that might ordinarily be considered to be systematic in nature. In fact, these covariance matrices can account for any error that increases the measurement residuals. That is, they will reflect any error that degrades the fit of the data to the VNA calibration error model. Some examples serve to illustrate this.

Probe-to-probe coupling in on-wafer calibrations depends on a number of factors, including the distance between the probes, and will change from measurement to measurement. The 12-term calibration model we use, which assumes static coupling, cannot correctly account for probe-to-probe coupling. Thus, coupling in the measurements will give rise to measurement residuals that will be accounted for in Σ_{CAL}, Σ_{DUT}, and $\Sigma_{\mathrm{CAL+DUT}}$.

Errors in the definition of the lengths of the open and short standards used in a short–open–load–thru (SOLT) calibration are typically considered systematic errors that must be imported into the calibration. However, if we use a number of shorts and opens with different errors in their length definitions, these differences will manifest themselves as a lack of fit of the calibration data to the VNA calibration model, and increase the measurement residuals. Here, again, the algorithm will automatically detect and account for these errors in standard definitions.

Thus, we see that, in fact, the type-A uncertainties we determined automatically account for a number of error mechanisms that would normally be considered systematic in nature. This means that only a relatively small number of additional systematic type-B uncertainties need be imported into the error analysis.

B. Systematic Type-B Uncertainties

We cannot, however, estimate all measurement uncertainties from measurement residuals. For example, in TRL calibrations, we calculate the characteristic impedance of the transmission-line standards from $\varepsilon_{\mathrm{eff}}$ and a user-supplied capacitance per unit length of line. Errors in the user-supplied capacitance change the reference impedance of the calibration. However, a calibration with a different reference impedance is still a solution to the calibration problem so the error in reference impedance does not manifest itself as a lack of fit of the measurements to the calibration model. Since this reference impedance error does not affect the measurement residuals, this systematic error will not be accounted for in the type-A uncertainties we considered above.

Consider also our previous SOLT example. If the offsets in the definitions of the lengths of the opens or shorts were all positive on one port and all negative on the other port, this would result in a shift of the calibration reference plane. However, this new calibration still corresponds to a solution of the calibration problem with a shifted reference plane so, again, the systematic error in the reference-plane position of the calibration does not affect the measurement residuals.

In cases like these, where systematic errors in standard definitions do not increase the measurement residuals, we must find another way to incorporate these errors into our uncertainty estimates. To do this, we construct a covariance matrix Σ_{SYST} from simple electrical models to describe the systematic errors.

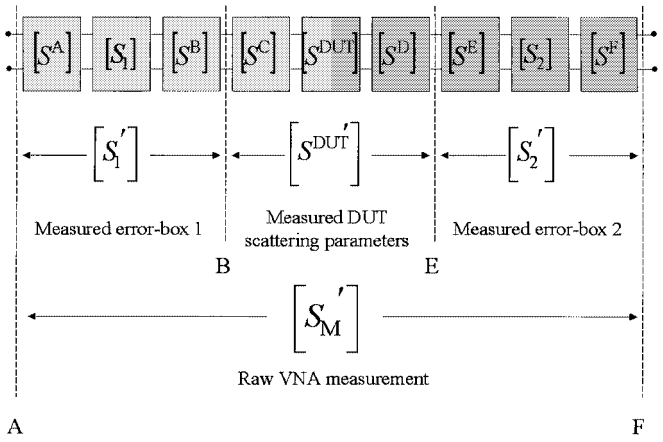

Fig. 3. Sketch of the error model describing the systematic uncertainties.

Our implementation of the algorithm supports several electrical models defined by a single parameter that describe reference impedance, reference plane, and series inductance errors that the user can easily "import" into the uncertainty analysis. The algorithm also supports more general sets of systematic errors defined by user-supplied covariance matrices describing the error sources. Once the covariance matrices defining these error sources have been defined, the algorithm translates them into uncertainties in the results using Jacobian matrices.

We describe these systematic errors with an error-box model that equally distributes errors on the two measurement ports. We not only assume that the errors represented by the error boxes are small so that second-order error terms can be neglected, but that the error boxes are reciprocal, i.e., we assume that the forward and reverse transmission coefficients of the error boxes are equal. This is reasonable not only because power-normalized scattering parameters describing typical systematic errors corresponding to real reference impedance transformations, reference plane transformations, and parasitic lumped elements are reciprocal [12], but also because any error that creates asymmetry in the forward and reverse transmission coefficients would give rise to measurement residuals that would be detected and included in our type-A uncertainties.

Fig. 3 sketches the error model we use to describe these imported systematic errors. The components of the model labeled $[S_1]$, $[S^{\mathrm{DUT}}]$, and $[S_2]$ correspond, respectively, to the true scattering parameters of the first error box, DUT, and second error box. The components labeled $[S^A]$, $[S^B]$, $[S^C]$, $[S^D]$, $[S^E]$, and $[S^F]$ correspond to the error boxes describing the systematic errors.

The measured scattering parameters $[S_1']$ of the first error box in Fig. 3 correspond to the cascade of the systematic error $[S^A]$, the true scattering parameters $[S_1]$ of the error box, and the systematic errors $[S^B]$. Likewise, the measured scattering parameters $[S_2']$ of the second error box correspond to the cascade of the systematic error $[S^E]$, the true scattering parameters $[S_2]$ of the error box, and the systematic errors $[S^F]$. Finally, the measured scattering parameters $[S^{\mathrm{DUT}\prime}]$ of the DUT correspond to the cascade of the systematic error $[S^C]$, the true scattering parameters $[S^{\mathrm{DUT}}]$ of the DUT, and the systematic errors $[S^D]$.

To add a systematic error to our uncertainty analysis, we begin by writing down the scattering parameters ΔS_{11}, ΔS_{22}, and $1 + \Delta S_{21}$ of the error box that models the source of the error we wish to include. For example, to model an error in a reference-plane transformation, $\Delta S_{11} = \Delta S_{22} = 0$ and $\Delta S_{12} = \Delta S_{21} = j\Delta\theta$, where $\Delta\theta$ is the error in the reference-plane position in radians.

Next, we use a first-order error-propagation analysis to express $[S^A]$ and $[S^F]$ or $[S^B]$, $[S^C]$, $[S^D]$, and $[S^E]$ depending on the reference plane at which the systematic errors are located, in terms of ΔS_{11}, ΔS_{22}, and ΔS_{21}. It is evident that, if the error occurs in the first tier of a two-tier calibration (the two outer reference planes A and F of Fig. 3), $[S^A]$ and $[S^F]$ are

$$[S^A] = \begin{bmatrix} \Delta S_{11} & 1+\Delta S_{21} \\ 1+\Delta S_{21} & \Delta S_{22} \end{bmatrix} \tag{5}$$

and

$$[S^F] = \begin{bmatrix} \Delta S_{22} & 1+\Delta S_{21} \\ 1+\Delta S_{21} & \Delta S_{11} \end{bmatrix} \tag{6}$$

where we have deliberately reversed the indexes of ΔS_{11} and ΔS_{22} in (6).

The indexes in (6) are reversed to account for the fact that port 1 of $[S^A]$ faces toward the analyzer, while port 1 of $[S^F]$ faces away from the analyzer. However, if we wish to use a single model to represent the errors on both sides of the DUT, port 1 of the model must always face toward the network analyzer and port 2 of the model must always face away from the analyzer. Thus, reversing the indexes in this way allows us to use a single model and representation for the errors at the two ports in terms of ΔS_{11}, ΔS_{22}, and ΔS_{21}, and simplifies the notation.

If the error occurs in a first-tier calibration or in the second tier of a two-tier calibration (the two inner reference planes B and E of Fig. 3), $[S^B]$, $[S^C]$, $[S^D]$, and $[S^E]$ are given by

$$[S^B] = \begin{bmatrix} \Delta S_{11} & 1+\Delta S_{21} \\ 1+\Delta S_{21} & \Delta S_{22} \end{bmatrix} \tag{7}$$

$$[S^C] = \begin{bmatrix} -\Delta S_{11} & 1-\Delta S_{21} \\ 1-\Delta S_{21} & -\Delta S_{22} \end{bmatrix} \tag{8}$$

$$[S^D] = \begin{bmatrix} -\Delta S_{22} & 1-\Delta S_{21} \\ 1-\Delta S_{21} & -\Delta S_{11} \end{bmatrix} \tag{9}$$

and

$$[S^E] = \begin{bmatrix} \Delta S_{22} & 1+\Delta S_{21} \\ 1+\Delta S_{21} & \Delta S_{11} \end{bmatrix} \tag{10}$$

where again the indexes in (10) are intentionally reversed.

The negative signs in (8) and (9) ensure that the systematic errors introduced into the scattering parameters of the DUT properly reflect the systematic errors in the error boxes that gave rise to them. We can derive the form of (8) and (9) from the following argument.

Imagine that there are no errors at the outer two reference planes in the model of Fig. 3. The cascade matrices $[T^A]$ and $[T^B]$, where $[T^X]$ is the cascade matrix corresponding to the scattering-parameter matrix $[S^X]$, will then be equal to identity matrices. In the absence of systematic errors at the two inner reference planes of Fig. 3, the cascade matrix $[T'_M]$ corresponding to the measurement $[S'_M]$ can be written as

$$[T'_M] = [T_1] \cdot [T^{\mathrm{DUT}}] \cdot [T_2]. \tag{11}$$

However, the addition of a systematic error at the inner reference planes of Fig. 3 does not change the measurement $[S'_M]$. Thus, the cascade matrix $[T'_M]$ corresponding to $[S'_M]$ can also be written as

$$\begin{aligned}[T'_M] &= [T'_1] \cdot [T^{\mathrm{DUT}'}] \cdot [T'_2] \\ &= [T_1] \cdot [T^B] \cdot [T^C] \cdot [T^{\mathrm{DUT}}] \\ &\quad \cdot [T^D] \cdot [T^E] \cdot [T_2]. \end{aligned} \tag{12}$$

Since both (11) and (12) must hold for any DUT, we see immediately that $[T^B] = [T^C]^{-1}$ and $[T^D] = [T^E]^{-1}$. Eliminating second-order terms in ΔS_{11}, ΔS_{22}, and ΔS_{21} leads directly to (8) and (9). This is convenient because once we have determined ΔS_{11}, ΔS_{22}, and ΔS_{21}, we know not only $[S^B]$ and $[S^E]$, but also $[S^C]$ and $[S^D]$.

While (5)–(10) describe the error boxes modeling systematic errors at the outer and inner reference planes, they do not capture the correlations between the elements of the error boxes or represent the errors and their correlations in a form convenient for computing the propagation of the errors into the solution vector β. To circumvent this problem, we use (5)–(10) to aid in the construction covariance matrices Σ_{AFi} and Σ_{BEi} to describe these errors and correlations.

Table II tabulates the elements of these covariance matrices corresponding to a systematic error in the reference-plane position at the first-tier reference planes A and F in Fig. 3 or the second-tier reference planes B and E in Fig. 3. In the uncertainty analysis, we treat the real and imaginary parts of each complex quantity as two real numbers so Σ_{AFi} and Σ_{BEi} are real 12-by-12 covariance matrices. The first row and column of Table II indicate the associated variable in the covariance matrix.

TABLE II
COVARIANCE MATRIX Σ_{AF} OR Σ_{BE} RELATING THE REAL AND IMAGINARY ELEMENTS OF $[S^A]$ AND $[S^F]$ OR $[S^B]$ AND $[S^E]$ FOR A SYSTEMATIC ERROR IN THE REFERENCE-PLANE POSITION. BLANK SPACES REPRESENT 2-BY-2 MATRICES FILLED WITH ZEROS. THE INDEXES P AND Q CAN BE REPLACED BY EITHER A AND F OR B AND E

Σ_{PQ}	S_{11}^P	S_{22}^P	S_{21}^P	S_{11}^Q	S_{22}^Q	S_{21}^Q
S_{11}^P						
S_{22}^P						
S_{21}^P			$\Delta\Theta$			$\pm\Delta\Theta$
S_{11}^Q						
S_{22}^Q						
S_{21}^Q			$\pm\Delta\Theta$			$\Delta\Theta$

Recall that, in this case, $\Delta S_{11} = \Delta S_{22} = 0$ and $\Delta S_{21} = j\Delta\theta$. Each entry in Table II corresponds to a 2-by-2 matrix, and blank spaces represent 2-by-2 matrices filled with zeros. Since $\Delta S_{11} = \Delta S_{22} = 0$, any row or column associated with these reflection coefficients are filled with zeros.

The symbol $\Delta\Theta$ in Table II is defined by

$$\Delta\Theta \equiv \begin{bmatrix} 0 & 0 \\ 0 & \Delta\theta^2 \end{bmatrix} \tag{13}$$

TABLE III
JACOBIAN MATRIX $\boldsymbol{J}_{AF}$ MAPPING THE Σ_{AFi} INTO Σ_{SYST}

$\boldsymbol{J}_{\mathrm{AF}}$	$S_{11}{}^{\mathrm{A}}$	$S_{22}{}^{\mathrm{A}}$	$S_{21}{}^{\mathrm{A}}$	$S_{11}{}^{\mathrm{F}}$	$S_{22}{}^{\mathrm{F}}$	$S_{21}{}^{\mathrm{F}}$
$S_{1,11}$	1	$(S_{1,11})^2$	$2\,S_{1,11}$			
$S_{1,22}$		$(S_{1,21})^2$				
$S_{1,21}$		$S_{1,11}$	$S_{1,21}$			
$S_{2,11}$					$(S_{2,21})^2$	
$S_{2,22}$				1	$(S_{2,22})^2$	$2\,S_{2,22}$
$S_{2,21}$					$S_{2,22}$	$S_{2,21}$
$S_{11}{}^{\mathrm{DUT}}$						
$S_{22}{}^{\mathrm{DUT}}$						
$S_{21}{}^{\mathrm{DUT}}$						
$S_{12}{}^{\mathrm{DUT}}$						

TABLE IV
JACOBIAN MATRIX $\boldsymbol{J}_{BE}$ MAPPING THE Σ_{BEi} INTO Σ_{SYST}

$\boldsymbol{J}_{\mathrm{BE}}$	$S_{11}{}^{\mathrm{B}}$	$S_{22}{}^{\mathrm{B}}$	$S_{21}{}^{\mathrm{B}}$	$S_{11}{}^{\mathrm{E}}$	$S_{22}{}^{\mathrm{E}}$	$S_{21}{}^{\mathrm{E}}$
$S_{1,11}$	$(S_{1,21})^2$					
$S_{1,22}$	$(S_{1,22})^2$	1	$2\,S_{1,22}$			
$S_{1,21}$	$S_{1,22}$		$S_{1,21}$			
$S_{2,11}$				$-(S_{1,11})^2$	1	$2\,S_{2,11}$
$S_{2,22}$				$(S_{2,21})^2$		
$S_{2,21}$				$S_{2,11}$		$S_{2,21}$
$S_{11}{}^{\mathrm{DUT}}$	-1	$-(S_{11}{}^{\mathrm{DUT}})^2$	$-2\,S_{11}{}^{\mathrm{DUT}}$		$-S_{21}{}^{\mathrm{DUT}}\,S_{12}{}^{\mathrm{DUT}}$	
$S_{22}{}^{\mathrm{DUT}}$		$-S_{21}{}^{\mathrm{DUT}}\,S_{12}{}^{\mathrm{DUT}}$	$-2\,S_{22}{}^{\mathrm{DUT}}$	-1	$-(S_{22}{}^{\mathrm{DUT}})^2$	
$S_{21}{}^{\mathrm{DUT}}$		$-S_{11}{}^{\mathrm{DUT}}$	$-S_{21}{}^{\mathrm{DUT}}$		$-S_{22}{}^{\mathrm{DUT}}$	$-S_{21}{}^{\mathrm{DUT}}$
$S_{12}{}^{\mathrm{DUT}}$		$-S_{11}{}^{\mathrm{DUT}}$	$-S_{12}{}^{\mathrm{DUT}}$		$-S_{22}{}^{\mathrm{DUT}}$	$-S_{21}{}^{\mathrm{DUT}}$

where $\Delta\theta^2$ corresponds to the square of the standard uncertainty in $\Delta\theta$. The two 2-by-2 matrices $\Delta\Theta$ on the diagonal of the covariance matrix Σ_{PQ}, with PQ equal to AF or BE, as appropriate, correspond to the standard uncertainties in the imaginary part of ΔS_{21}, while the off-diagonal matrices $\pm\Delta\Theta$ in Σ_{PQ} describe the correlations between the imaginary part of ΔS_{21} at reference planes P and Q. The positive sign is used for positively correlated reference-plane-position shifts (i.e., the two reference planes move toward and away from the analyzer together), the negative sign is used for negatively correlated reference-plane-position shifts (i.e., the two reference planes move left and right together), and $\pm\Delta\Theta$ is set to zero for uncorrelated reference-plane-position shifts.

We see from this analysis that the covariance matrices Σ_{AFi} and Σ_{BEk} describing the sources of systematic error must be constructed individually. For this reason, we have hard-coded covariance matrices describing reference-plane position and reference-impedance errors, as well as systematic errors due to series inductances at the measurement port, as often arises in coaxial TRL calibrations. Reference [16] offers useful explanations useful for constructing custom covariance matrices to describe other systematic errors not already hard coded into the algorithm.

After constructing Σ_{AFi} and Σ_{BEk}, we use closed-form Jacobian matrices $\boldsymbol{J}_{AF}$ and $\boldsymbol{J}_{BE}$ derived from a first-order error propagation analysis to translate the errors described in Σ_{AFi} and Σ_{BEk} into a covariance matrix Σ_{SYST} describing the uncertainties in the solution vector β via

$$\Sigma_{\mathrm{SYST}} = \sum_i \left(J_{AF}\Sigma_{AFi}J_{AF}^T\right) + \sum_k \left(J_{BE}\Sigma_{BEk}J_{BE}^T\right). \tag{14}$$

Since the Jacobian matrices $\boldsymbol{J}_{AF}$ and $\boldsymbol{J}_{BE}$ map the errors described in the 12-by-12 covariance matrices Σ_{AFi} and Σ_{BEk} into the covariance matrix Σ_{SYST}, which has the same dimension as the solution vector β, $\boldsymbol{J}_{AF}$ and $\boldsymbol{J}_{BE}$ have 12 columns and a number of rows equal to the dimension of the solution vector β. Once formed, the covariance matrix Σ_{SYST} includes the effects of the systematic errors on both the calibration coefficients and scattering parameters of the DUT.

Tables III and IV give the Jacobians $\boldsymbol{J}_{AF}$ and $\boldsymbol{J}_{BE}$ that we use. How we order the elements of Σ_{AFi}, Σ_{BEk}, and Σ_{SYST} is a matter of convention. The elements in the first row of the tables refer to the ordering we used for Σ_{AF} and Σ_{BE}, the covariance matrices describing the circuit-level description of the systematic errors. The elements of the first column of the tables refer to the ordering we used for Σ_{SYST}, the covariance matrix describing the effect of the systematic errors on the solution vector after they are mapped from Σ_{AF} and Σ_{BE}.

The function of $\boldsymbol{J}_{AF}$ and $\boldsymbol{J}_{BE}$ is to map the errors contained in $[S^A]$, $[S^B]$, $[S^C]$, $[S^D]$, $[S^E]$, and $[S^F]$ into Σ_{SYST}. $\boldsymbol{J}_{AF}$ and $\boldsymbol{J}_{BE}$ can be constructed by a simple first-order analysis in the

errors contained in $[S^A]$, $[S^B]$, $[S^C]$, $[S^D]$, $[S^E]$, and $[S^F]$ by writing down the scattering parameters of $[S'_1]$, $[S'_2]$, and $[S'_{\rm DUT}]$ (see Fig. 3) in terms of $[S^A]$, $[S^B]$, $[S^C]$, $[S^D]$, $[S^E]$, $[S^F]$, $[S_1]$, $[S_2]$, and $[S_{\rm DUT}]$. For example, to construct the first row of $\boldsymbol{J}_{AF}$ in Table III, we write $S'_{1,11}$ in terms of the reflection coefficient of the cascade of $[S^A]$ and $[S_1]$ as

$$\begin{aligned} S'_{1,11} &= S^A_{11} + \frac{S^A_{21}S^A_{21}}{1-S^A_{22}S_{1,11}} S_{1,11} \\ &\approx S^A_{11} + S_{1,11}\left(1+\left(S^A_{21}-1\right)\right) \\ &\quad \times \left(1+\left(S^A_{21}-1\right)\right)\left(1+S^A_{22}S_{1,11}\right) \\ &\approx S_{1,11} + S^A_{11} + (S_{1,11})^2 S^A_{22} + 2S_{1,11}\left(S^A_{21}-1\right). \end{aligned} \quad (15)$$

Thus, we see that a small error S^A_{11} contributes an equal error to $S'_{1,11}$ so $\boldsymbol{J}_{AF,11} = 1$. A small error S^A_{22}, on the other hand, contributes an error $(S_{1,11})^2 S^A_{22}$ to $S'_{1,11}$ so $\boldsymbol{J}_{AF,12} = (S_{1,11})^2$. Finally, a small error $(S^A_{21} - 1)$ in S^A_{21} contributes an error $2S_{1,11}(S^A_{21} - 1)$ to $S'_{1,11}$ so $\boldsymbol{J}_{AF,13} = 2S_{1,11}$.

Again, we treat the real and imaginary parts of each complex vector in the analysis as two real quantities so each entry in the tables actually corresponds to a 2-by-2 matrix of the form

$$\begin{bmatrix} a & -b \\ b & a \end{bmatrix} \quad (16)$$

where a is the real part of the complex quantity and b is its imaginary part. The blank spaces in the tables represent 2-by-2 matrices filled with zeros.

Note that $\boldsymbol{J}_{BE}$ has a number of elements not found in $\boldsymbol{J}_{AF}$. This is because $\boldsymbol{J}_{BE}$ not only maps the errors captured in $[S^B]$ and $[S^E]$ into the parts of $\Sigma_{\rm SYST}$ related to the uncertainties in the calibration coefficients, but also the errors captured in $[S^C]$ and $[S^D]$, which contribute to the uncertainty in the DUT. Formulating the problem in this way is extremely convenient for the user, who need only specify Σ_{BE} to translate all of the errors captured in ΔS_{11}, ΔS_{22}, and ΔS_{21} and their correlations into uncertainties and correlations in the entire solution vector, including those related to the DUT.

C. Combined Uncertainty

The algorithm reports a combined standard uncertainty described by the covariance matrix $\Sigma_{\rm SYST+CAL+DUT} = \Sigma_{\rm SYST} + \Sigma_{\rm CAL+DUT}$. This covariance matrix describes both the type-A and the type-B uncertainties and their correlations in the combined calibration/DUT solution. The diagonal elements of $\Sigma_{\rm SYST+CAL+DUT}$ contain the square of the standard uncertainties of each of the measured calibration and DUT parameters, which we can represent either as real-imaginary or in-phase-quadrature pairs.

Fig. 4 plots the combined standard uncertainty $s_{\rm SYST+CAL+DUT}$ of the quadrature component of the transmission coefficient of a DUT calibrated with a TRL calibration obtained from the in-phase/quadrature representation of $\Sigma_{\rm SYST+CAL+DUT}$ as a solid line. This figure also plots the standard uncertainty $s_{\rm DUT}$ obtained from $\Sigma_{\rm DUT}$ and the standard uncertainty $s_{\rm CAL+DUT}$ obtained from $\Sigma_{\rm CAL+DUT}$.

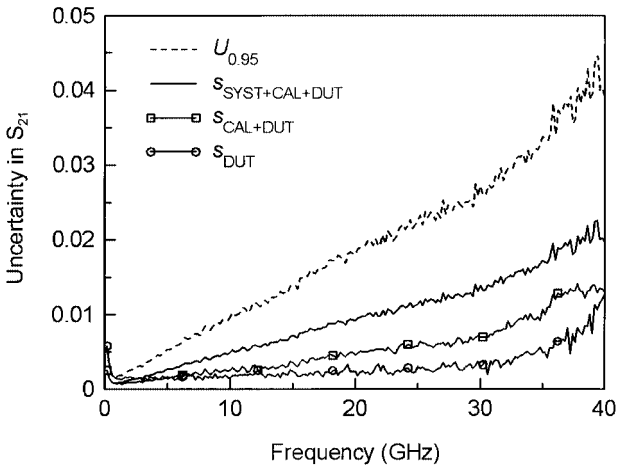

Fig. 4. Components of quadrature uncertainty in S_{12} for a DUT as a function of frequency. The quadrature uncertainty is in a direction perpendicular to the direction of S_{12}.

D. Expanded Uncertainty

We determine expanded uncertainties $U_{0.95}$, defining the 95% confidence intervals associated with each component of the solution, from a set of "one-at-a-time coverage factors" $k_{0.95}$. Multiplying the standard uncertainty $s_{\rm SYST+CAL+DUT}$ by the coverage factor $k_{0.95}$ gives the expanded uncertainty $U_{0.95}$ (see Fig. 4). We have a 95% confidence that the true value of a solution parameter is in the interval defined by the reported value $\pm U_{0.95}$ [16].

We calculate $k_{0.95}$ separately for each component of the solution vector β from the effective number of degrees of freedom $\nu_{\rm eff}$ associated with that element of the solution using the Welch–Satterthwaite formula [16]. For the calibration parameters, we estimate $\nu_{\rm eff}$ as

$$\nu_{\rm eff} = \frac{\left(s^2_{\rm CAL} + s^2_{\rm SYST}\right)^2}{\dfrac{s^4_{\rm CAL}}{\nu_{\rm CAL}} + \dfrac{s^4_{\rm SYST}}{\nu_{\rm SYST}}}. \quad (17)$$

For the DUTs, we estimate $\nu_{\rm eff}$ as

$$\nu_{\rm eff} = \frac{\left(s^2_{\rm CAL} + s^2_{\rm DUT} + s^2_{\rm SYST}\right)^2}{\dfrac{s^4_{\rm CAL}}{\nu_{\rm CAL}} + \dfrac{s^4_{\rm DUT}}{\nu_{\rm DUT}} + \dfrac{s^4_{\rm SYST}}{\nu_{\rm SYST}}} \quad (18)$$

where we estimate $s^2_{\rm CAL}$ as $s^2_{\rm CAL+DUT} - s^2_{\rm DUT}$ when $s^2_{\rm CAL+DUT} - s^2_{\rm DUT}$ is positive, and as zero otherwise. This is because when the true value of the uncertainty due to the calibration is small compared to the true value of the uncertainty due to the DUT, there is a nonnegligible probability that $s^2_{\rm CAL+DUT} < s^2_{\rm DUT}$. In such cases, without additional information, we set $s_{\rm CAL} = 0$.

We determine the number of degrees of freedom $\nu_{\rm CAL}$ and $\nu_{\rm DUT}$ in (17) and (18) as the number of measured real values in the calibration and DUT problems minus the number of real values we solve for in those problems after accounting for any deficiencies in the rank of the solution. By default, we set the number of degrees of freedom $\nu_{\rm SYST}$ associated with the systematic errors to infinity, although the user may override this default.

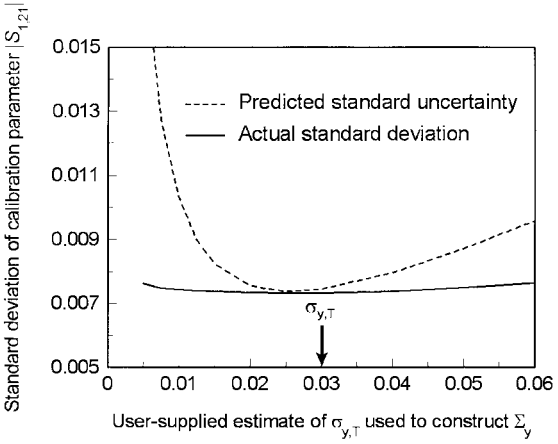

Fig. 5. Actual and predicted standard deviations of the calibration parameter $|S_{1,21}|$ as a function of the user-supplied estimate of $\sigma_{y,T}$ used to construct Σ_y with $s_{y,R} = \sigma_{y,R} = 0.01$.

Finally, we determine $k_{0.95}$ from $t_{0.95}(\nu_{\text{eff}})$, where t represents the student's t-distribution [16]. Fig. 4 plots $U_{0.95} = k_{0.95}s_{\text{CAL+DUT+SYST}}$ as a dashed line. Since all of the degrees of freedom were at least 40 for the calibration problem of Fig. 4, $k_{0.95} \approx 2$ in Fig. 4.

E. Re-Weighting

As we explained earlier, the algorithm can make use of user-supplied block-diagonal covariance matrices Σ_y describing the errors in the raw network-analyzer measurements and Σ_x describing the errors in the calibration-standard definitions. The algorithm uses Σ_y and Σ_x to determine the relative weights w_ε and w_δ that it uses to find solutions, and to estimate the uncertainties in its results. In this section, we will discuss the effect of the user-supplied estimates in Σ_y on the solution and the uncertainty the algorithm predicts for that solution, as well as a strategy for verifying and refining user-supplied estimates.

In the on-wafer test case we discussed in Section V, we added error with a standard deviation $\sigma_{y,R}$ of 0.01 into the simulated reflection-coefficient measurements and standard deviation $\sigma_{y,T}$ of 0.03 into the simulated transmission-coefficient measurements. To illustrate ideas, we constructed a diagonal Σ_y matrix from user-supplied estimates $s_{y,R}$ and $s_{y,T}$ of $\sigma_{y,R}$ and $\sigma_{y,T}$. Fig. 5 illustrates the effect of the user's estimates $s_{y,T}$ on the solution for the calibration parameter $|S_{1,21}|$ and the uncertainty in $|S_{1,21}|$ the algorithm predicts with $s_{y,R} = \sigma_{y,R} = 0.01$.

The solid line in Fig. 5 shows the standard deviation of the error in the calibration parameter $|S_{1,21}|$. This figure shows that the algorithm's solution accuracy is a very weak function of the user-supplied estimate $s_{y,T}$ used to construct Σ_y.

The dashed line in Fig. 5 shows the standard uncertainty of $|S_{1,21}|$ estimated by the algorithm. This figure shows that the algorithm's estimate of its own uncertainty improves measurably when the user-supplied estimate $s_{y,T}$ approaches the actual value of $\sigma_{y,T} = 0.03$ marked by the arrow in the figure. This demonstrates that there is a small, but tangible, advantage to be gained in the accuracy of the algorithms uncertainty predictions by accurately estimating Σ_y and Σ_x.

The covariance matrix Σ_x can usually be estimated from dimensional tolerances, electrical models, or other physical parameters of the calibration standards. However, the elements of the covariance matrix Σ_y that describes the uncertainty in the raw network-analyzer measurements will vary from instrument to instrument and measurement setup to measurement setup.

We developed a verification and refinement procedure to address this problem based on a comparison of the measurement residuals detected by the algorithm with the user-supplied estimates of those residuals. To perform the comparison, the algorithm determines the standard deviations $\sigma_{\varepsilon,T}$ and $\sigma_{\varepsilon,R}$ of the elements of the residuals ε_i of the solution associated with the raw measured reflection and transmission coefficients based on the user supplied estimates of $s_{y,R}$ and $s_{y,T}$ of $\sigma_{y,R}$ and $\sigma_{y,T}$. These standard deviations $\sigma_{\varepsilon,T}$ and $\sigma_{\varepsilon,R}$ reflect the actual lack-of-fit of the raw measurements to the calibration model based on the user's initial estimates $s_{y,R}$ and $s_{y,T}$. This allows the user to compare the user-defined estimates $s_{y,R}$ and $s_{y,T}$ to the actual measurement residuals, refine the estimates $s_{y,R}$ and $s_{y,T}$, and resolve the problem with a set of optimized covariance matrices Σ_y and Σ_x and weights that better correspond to the actual instrument and measurement setup.

Our on-wafer test case illustrates that by using uniform weighting $(s_{y,T} = s_{y,R} = 0.01)$ for our on-wafer test case, the standard deviation of the residuals $\sigma_{\varepsilon,T}$ and $\sigma_{\varepsilon,R}$ associated with the transmission and reflection coefficients were 0.0277 and 0.0088, respectively. These estimates are quite close to the actual standard deviations $\sigma_{y,T} = 0.03$ and $\sigma_{y,R} = 0.01$ of the measurement error we added into these transmission measurements in the Monte Carlo simulation (see Fig. 5). In fact, Fig. 5 shows that results based on weights derived from setting $s_{y,T} = 0.0277$ are nearly identical to those obtained based on the actual value of $\sigma_{y,T} = 0.03$, and demonstrate nicely the utility of this re-weighting scheme.

Although our first cycle of refinement of the estimates of $s_{y,T}$ and $s_{y,R}$ were quite good, in some situations, it might be possible to iterate on $s_{y,T}$ and $s_{y,R}$ to improve on these estimates. We tested this by adjusting $s_{y,T}$ and $s_{y,R}$ to 0.0277 and 0.0088, and recalculating the residuals. We then obtained similar estimates $\sigma_{\varepsilon,T} = 0.0283$ and $\sigma_{\varepsilon,R} = 0.00982$ for $\sigma_{y,T}$ and $\sigma_{y,R}$. This indicates to the user that no further improvement is to be gained in this example with more refinement iterations.

IX. Conclusion

We have presented an iterative algorithm based on orthogonal distance regression for performing VNA calibrations. The algorithm allows a flexible "mix and match" approach to VNA calibrations that takes into account the relative accuracy in the calibration standards and the relative accuracy in the measurements to arrive at an optimal calibration solution.

The algorithm is not intended to replace traditional error analyses based on a history of check-standard measurements and the application of standard statistical methods to separately determine uncertainty due to repeatability and reproducibility. These more standard approaches will most likely always result in the most reliable uncertainty estimates possible. However, this algorithm offers an easy-to-implement alternative that

automatically estimates the uncertainty in the calibration due to most error sources from measurement residuals, and allows any remaining systematic errors to be readily added to the overall uncertainty estimate.

APPENDIX
SUPPORTED CALIBRATION STANDARDS

Our implementation supports the wide variety of calibration standards and DUTs listed below. As long as there are enough calibration standards with which to solve the problem, any of the calibration standards can be "mixed and matched" with any other calibration standards, allowing great flexibility in the choice of calibration strategy. The weights w_ε are based on the estimated accuracy of the measurements, while the weights w_δ are used to account for differences in the relative accuracy of the various standards in any given calibration.

A. Thru Calibration Standard

The thru calibration standard is realized by forming a zero-length connection at the calibration reference plane. The scattering parameters of the thru standard are, by definition, $S_{11} = S_{22} = 0$ and $S_{21} = S_{12} = 1$. Translating the reference plane in the calibration usually requires defining the thru standard as a transmission line of either positive or negative length.

B. Transmission-Line Calibration Standard

The characteristic impedance of the transmission-line standard supported by the algorithm is determined from a user-supplied capacitance per unit length, and is assumed to be constant. This is explained in [17] and [18]. The scattering parameters of the transmission-line standard are calculated with respect to a reference impedance of 50 Ω. As a result, the reference impedance of calibrations using these line standards is set to 50 Ω.

The algorithm also allows the reference impedance of the scattering parameters of the line standards to be set to the characteristic impedance of the transmission-line standard to support calibrations with reference impedance equal to the characteristic impedance of the line.

C. Reflect Calibration Standard

The reflect calibration standard supported by the algorithm has equal, but unknown reflection coefficients at each port, and no transmission. Adding a reflect standard to a calibration requires adding its reflection coefficient Γ_r to the solution vector. The algorithm thus supports only a single reflect in each calibration, although it may be measured many times. While the reflect is essential for setting the reference plane in TRL calibrations, the algorithm can support the reflect standard in any calibration.

D. Load Calibration Standard

The algorithm supports a load calibration standard with known, but possibly different reflection coefficients at each port, and no transmission between its ports. This standard is used for adding shorts, opens, and resistors in SOLT calibrations and adding the match standard in line–reflect–match (LRM) calibrations. The load calibration standard with appropriate weighting can also be used in TRL calibrations to allow resistors to more accurately set the calibrations reference impedance at low frequencies or even to augment the TRL calibration with well-characterized shorts and opens over part or all of the frequency band.

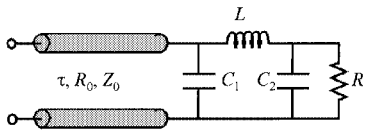

Fig. 6. Model used to describe the impedance of load calibration standards.

The reflection coefficients of the load can be defined from data in a file or with the analytic model of Fig. 6. The transmission line is defined by a delay τ_0, a resistance per unit length R_0, and a real characteristic impedance Z_0. For consistency with common industrial practice, we use a third-order Taylor-series expansion to describe the values of the lumped elements in Fig. 6. This analytical model is a superset of the most common coaxial standard definitions and of the on-wafer load definitions described in [19].

E. Reciprocal-Adapter Calibration Standard

The reciprocal-adapter calibration standard supported by the algorithm has unknown reflection and transmission coefficients. However, S_{21} must equal S_{12}. This standard is useful when calibrating with an adapter matching different transmission media at its two ports. The algorithm determines the unknown scattering parameters of the reciprocal adapter during the calibration procedure.

Adding a reciprocal-adapter standard to a calibration requires adding its two reflection coefficients and single transmission coefficient to the solution vector. The algorithm thus supports only a single reciprocal-adapter standard in each calibration, although it may be measured many times.

F. Attenuator Calibration Standard

All of the scattering parameters of the attenuator must be known, and its forward and reverse transmission coefficients must be equal. The scattering parameters of the attenuator can be defined from data in a file or by the transmission-line model of Fig. 6 defined by a delay τ_0, a resistance per unit length R_0, and a real characteristic impedance Z_0.

G. DUTs

To keep the number of unknowns in the solution vector β to an absolute minimum, the algorithm supports three types of DUTs, i.e., DUTs with unknown reflection coefficients and no transmission, reciprocal DUTs with unknown reflection coefficients and unknown, but equal forward and reverse transmission coefficients, and DUTs with unknown reflection and transmission coefficients.

SOFTWARE

The *StatistiCAL* software package implementing the method described here can be downloaded online.[3]

[3][Online]. Available: http://www.boulder.nist.gov/dylan/

ACKNOWLEDGMENT

The authors thank M. Janezic, J. Koontz, A. O'Gallagher, B. Alpert, R. Teichmann, and W. Morrison, for assistance with the programming and implementation, and J. Juroshek, R. Ginley, and R. Judish, all of NIST, for many helpful discussions.

REFERENCES

[1] D. F. Williams, C. M. Wang, and U. Arz, "An optimal multiline TRL calibration algorithm," in *IEEE MTT-S Int. Microwave Symp. Dig.*, June 2003, pp. 1819–1822.

[2] R. B. Marks, "A multiline method of network analyzer calibration," *IEEE Trans. Microwave Theory Tech.*, vol. 39, pp. 1205–1215, July 1991.

[3] D. F. Williams, "De-embedding and unterminating microwave test fixtures with nonlinear least squares," *IEEE Trans. Microwave Theory Tech.*, vol. 38, pp. 787–791, June 1990.

[4] R. M. Judish and G. F. Engen, "On-line accuracy assessment for the dual six-port ANA: Statistical methods for random errors," *IEEE Trans. Instrum. Meas.*, vol. IM-36, pp. 507–513, June 1987.

[5] H. Van Hamme and M. Vanden Bossche, "Flexible vector network analyzer calibration with accuracy bounds using an 8-term or a 16-term error correction model," *IEEE Trans. Microwave Theory Tech.*, vol. 42, pp. 976–987, June 1994.

[6] W. Van Moer and Y. Rolain, "Calibration of a wideband IF nonlinear vectorial network analyzer," in *53rd ARFTG Conf. Dig.*, June 1999, pp. 98–103.

[7] D. F. Williams, "Calibration in multiconductor transmission lines," in *48th ARFTG Conf. Dig.*, Orlando, FL, Dec. 4–6, 1996, pp. 46–53.

[8] D. F. Williams, "Multiconductor transmission line characterization," *IEEE Trans. Comp., Packag., Manufact. Technol. B*, vol. 20, pp. 129–132, May 1997.

[9] D. F. Williams, J. E. Rogers, and C. L. Holloway, "Multiconductor transmission line characterization: Representations, approximations, and accuracy," *IEEE Trans. Microwave Theory Tech.*, vol. 47, pp. 403–409, Apr. 1999.

[10] U. Arz, D. F. Williams, D. K. Walker, and H. Grabinski, "Asymmetric coupled CMOS lines: An experimental study," *IEEE Trans. Microwave Theory Tech.*, vol. 48, pp. 2409–2414, Dec. 2000.

[11] P. T. Boggs, R. H. Byrd, J. E. Rogers, and R. B. Schnabel, "User's reference guide for ODRPACK version 2.01 software for weighted orthogonal distance regression," NIST, Boulder, CO, Internal Rep. NISTIR 92-4834, June 1992.

[12] R. B. Marks and D. F. Williams, "A general waveguide circuit theory," *J. Res. Nat. Inst. Stand. Technol.*, vol. 97, pp. 533–562, 1992.

[13] W. H. Press, B. P. Flannery, S. A. Teukolsky, and W. T. Vetterling, *Numerical Recipes*. Cambridge, U.K.: Cambridge Univ. Press, 1986.

[14] D. Rytting, "An analysis of vector measurement accuracy enhancement techniques," presented at the RF and Microwave Symp. Exhibition, 1980.

[15] R. B. Marks, "Formulation of the basic vector network analyzer error model including switch terms," in *50th ARFTG Conf. Dig.*, Dec. 4–5, 1997, pp. 115–126.

[16] B. N. Taylor and C. E. Kuyatt, "Guidelines for evaluating and expressing the uncertainty of NIST measurement results," NIST, Boulder, CO, Tech. Note 1297, 1994.

[17] R. B. Marks and D. F. Williams, "Characteristic impedance determination using propagation constant measurement," *IEEE Microwave Guided Wave Lett.*, vol. 1, pp. 141–143, June 1991.

[18] D. F. Williams and R. B. Marks, "Transmission line capacitance measurement," *IEEE Microwave Guided Wave Lett.*, vol. 1, pp. 243–245, Sept. 1991.

[19] D. K. Walker, D. F. Williams, and J. M. Morgan, "Planar resistors for probe station calibration," in *40th ARFTG Conf. Dig.*, Dec. 1–9, 1992.

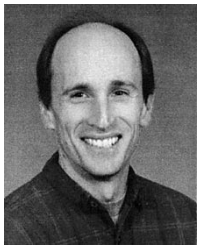

Dylan F. Williams (M'80–SM'90–F'02) received the Ph.D. degree in electrical engineering from the University of California at Berkeley, in 1986.

In 1989, he joined the Electromagnetic Fields Division, National Institute of Standards and Technology (NIST), Boulder, CO, where he develops metrology for the characterization of monolithic microwave integrated circuits and electronic interconnects. He has authored or coauthored over 80 technical papers.

Dr. Williams is an associate editor for the IEEE TRANSACTIONS ON MICROWAVE THEORY AND TECHNIQUES. He was the recipient of the Department of Commerce Bronze and Silver Medals, the Electrical Engineering Laboratory's Outstanding Paper Award, two ARFTG Best Paper Awards, the ARFTG Automated Measurements Technology Award, and the IEEE Morris E. Leeds Award.

Jack C. M. Wang received the Ph.D. degree in statistics from Colorado State University, Fort Collins, in 1978.

He is currently a Mathematical Statistician with the Statistical Engineering Division, National Institute of Standards and Technology (NIST), Boulder, CO. His research interests include interval estimation on variance components, statistical graphics and computing, and the application of statistical methods to physical sciences.

Dr. Wang is a Fellow of the American Statistical Association.

Uwe Arz (S'97–M'02) received the Dipl.-Ing. degree in electrical engineering and Ph.D. degree (*summa cum laude*) from the University of Hannover, Hannover, Germany, in 1994 and 2001, respectively.

From 1995 to 2001, he was a Research and Teaching Assistant with the Laboratory of Information Technology, University of Hannover. In 2001 he was a Post-Doctoral Research Associate with the National Institute of Standards and Technology (NIST), Boulder, CO. In 2002, he joined the Physikalisch-Technische Bundesanstalt (PTB), Braunschweig, Germany, where he develops metrology for on-wafer measurements.

Dr. Arz serves on the IEEE Microwave Theory and Techniques Society (IEEE MTT-S) Technical Committee on Microwave Measurements MTT-11 and is a member of the Technical Program Committee (TPC) of the 2004 Conference on Precision Electromagnetic Measurements. He was the recipient of the first ARFTG Microwave Measurement Student Fellowship Award in 1999 and the 2003 AHMT Measurement Award presented by the Association of German University Professors for Measurement Science.